

PAPER

## Characterizations of gas purge valves for liquid alignment and gas removal in a microfluidic chip

To cite this article: Han-Sheng Chuang *et al* 2012 *J. Micromech. Microeng.* **22** 085023

View the [article online](#) for updates and enhancements.

### You may also like

- [Effect of Electrochemical Oxidation Processes on Acetaminophen Degradation in Various Electro-Fenton Reactors](#)  
Chia-Chi Su, Crisanto A. Cada, Maria Lourdes P. Dalida et al.
- [Accumulation and Removal of Liquid Water in Proton Exchange Membrane Fuel Cells](#)  
Jon P. Owejan, Jeffrey J. Gagliardo, Steven R. Falta et al.
- [Moisture Uptake and Outgassing in Patterned and Capped Porous Low- \$k\$  Dielectric Films](#)  
Junpin Yao, Asad Iqbal, Harpreet Juneja et al.



The Electrochemical Society  
Advancing solid state & electrochemical science & technology

242nd ECS Meeting

Oct 9 – 13, 2022 • Atlanta, GA, US

**Extended abstract submission deadline: April 22, 2022**

Connect. Engage. Champion. Empower. Accelerate.

**MOVE SCIENCE FORWARD**



Submit your abstract



# Characterizations of gas purge valves for liquid alignment and gas removal in a microfluidic chip

Han-Sheng Chuang<sup>1,2</sup>, Raviraj Thakur<sup>3</sup> and Steven T Wereley<sup>3</sup>

<sup>1</sup> Department of Biomedical Engineering, National Cheng Kung University, Tainan, Taiwan

<sup>2</sup> Medical Device Innovation Center, National Cheng Kung University, Tainan, Taiwan

<sup>3</sup> Birck Nanotechnology Center and Mechanical Engineering, Purdue University, West Lafayette, IN, USA

E-mail: [oswaldchuang@mail.ncku.edu.tw](mailto:oswaldchuang@mail.ncku.edu.tw)


Received 3 April 2012, in final form 29 May 2012

Published 9 July 2012

Online at [stacks.iop.org/JMM/22/085023](http://stacks.iop.org/JMM/22/085023)

## Abstract

Two polydimethylsiloxane (PDMS) gas purge valves for excessive gas removal in general lab-on-a-chip applications are presented in this paper. Both valves are devised based on a three-layer configuration comprising a top layer for liquid channels, a membrane and a bottom layer for gas channels. The pneumatic valves work as a normal gateway for fluids when the membrane is bulged down (open state) by vacuum or pushed up (closed state) by pressure. In the closed state, the air in front of a liquid can be removed through a small notch or a permeable PDMS membrane by compressing the liquid. The purge valve with a small notch across its valve seat, termed surface-tension (ST) valve, can be operated with pressure under 11.5 kPa. The liquid is mainly retained by the surface tension resulting from the hydrophobic channel walls. In contrast, the purge valve with vacuum-filled grooves adjacent to a liquid channel, termed gas-permeation (GP) valve, can be operated at pressure above 5.5 kPa. Based on the principle of gas permeation, the excessive air can be slowly removed through the vent grooves. Detailed evaluations of both valves in a pneumatically driven microfluidic chip were conducted. Specifically, the purge valves enable users to remove gas and passively align liquids at desired locations without using sensing devices or feedback circuits. Finally, a rapid mixing reaction was successfully performed with the GP valves, showing their practicability as incorporated in a microfluidic chip.

 Online supplementary data available from [stacks.iop.org/JMM/22/085023/mmedia](http://stacks.iop.org/JMM/22/085023/mmedia)

(Some figures may appear in colour only in the online journal)

## Introduction

Excessive gas removal in microchannels is of great interest to lab-on-a-chip (LoC) applications, such as low mixing efficiency [17], poor temperature uniformity in PCR [13], or inhibitive reactions [8]. Because bubble formation is a typical issue commonly taking place in microchannels, unprocessed air bubbles or plugs may cause mass transport problems. As a result, excessive gas removal is usually regarded as a priority when dealing with microfluidic operations. With hydrophobic microcapillary vents [7], Lee *et al* [11] showed nanoliter metering, transportation, merging and biochemical reactions

on a microfluidic chip. Tiny liquid droplets were translated by low air pressure (<3.5 kPa) generated from vents. Similarly, residual air was removed through the vents. However, this device is only eligible for some limited circumstances due to the lack of physical valves. Another approach removing air bubbles through gas permeable PDMS channels was reported by Kang *et al* [9]. The concept relies on applying pressure over air/liquid phase flow to squeeze the air out of the liquid channel. The group successfully predicted the purge behavior with a gas permeable model and a correction factor. Urbanski *et al* [19] devised a latch valve to get rid of excessive mineral oil in oil/water flow for metering. Similar work can also be

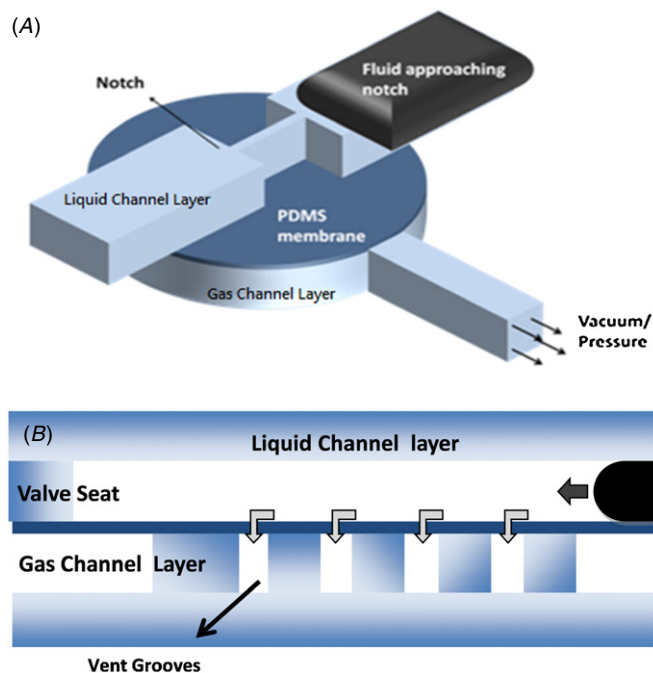


**Figure 1.** Schematic of the microfluidic gas purge valves. Both valves are operated under a closed state. (A) Surface-tension (ST) valve; (B) gas-permeation (GP) valve.

applied to air/liquid flow. This partially closed latch caught and retained emulsified aqueous samples, yet allowed the immiscible mineral oil to continuously flow along the channel. However, a pressure range different from the pressure acting on the normal valves has to be carefully adjusted to achieve the partially closed state. In addition, leakage is very likely to be a problem in the device. It is worth noting that removing air in microchannels also enables passive liquid alignment at a desired location without a sophisticated sensing system. In contrast, the past detections of fluid locations still relied on sensors based on the change of electrical signals [3, 14]. The additional capability therefore allows accurate dispensing as well as metering in many biochemical assays.

In this paper, we devised and characterized two types of gas purge valves based on the valve proposed by Mathies' group [5]. The three-layer pneumatic valve is used in a wide variety of LoC applications due to simplicity. In such a valve, a flexible membrane is sandwiched between two functional layers, isolating liquid channels and gas channels. A valve is defined 'closed' when the membrane seals a liquid channel but turns 'open' when the sealing state breaks. With multiple valves deployed in a microfluidic chip, one is able to handle sophisticated fluid behavior using programmable controls [6, 18]. In addition to the basic functions, a gas purge valve is designed to remove excessive gas from a liquid channel, thus preventing air bubbles and aligning liquids without sensors or feedback circuits. Two types of purge valves subjected to different operating mechanisms were fabricated and studied (see figure 1). The ST valve features a small notch on the valve seat and resists the fluid flow due to high surface tension. When surface tension dominates, the fluid interface will be retained at the notch valve. When the driving pressure is higher than the threshold, the

fluid will leak through the notch. For the current study, a notch with 150  $\mu\text{m}$  cumulative width and 4.66  $\mu\text{m}$  depth was designed to bear pressure under 11.5 kPa. The GP valve has several finger-like grooves adjacent to a liquid channel and is vacuum vented. As a result, it can work at pressure higher than 5.5 kPa. Since both the devices are on the basis of Mathies' valve, they can also be used as normal valves as long as being operated within the designed pressure ranges.

## Methods and materials

Both the purge valves were comprised of three layers of PDMS (Sylgard 184, Ellsworth Adhesives) structures: liquid channel, membrane and gas channel. The liquid and gas channels were fabricated using replica molding of PDMS with SU8 micromolds. For the GP valve, a standard single-step lithography procedure was followed using SU8 2025 (MicroChem). For the ST valve, fabricating a notch ( $\sim 4.5 \mu\text{m}$ ) in single-step lithography presented substantial challenges in terms of high aspect ratio features and necessitated high-resolution masks. Therefore, an alternative, called multilayer SU8 lithography protocol [12], was followed to create the desired notch. The notch was fabricated by spin-coating SU8 2002 at 500 rpm and the liquid channel layer was built on top of it using SU8 2025. Finally, both layers were developed simultaneously. The details of the process can be found in the supplementary material (available at [stacks.iop.org/JMM/22/085023/mmedia](http://stacks.iop.org/JMM/22/085023/mmedia)).

The PDMS prepolymer was prepared by mixing Sylgard 184 and cure agent in a ratio of 10:1. Conventional photolithography was used to fabricate SU8 2025 master micromolds for both the liquid and the gas channels. Both the PDMS layers were cast from the molds and cured in an oven at 65  $^{\circ}\text{C}$  for 1 h. A membrane was fabricated by spin-coating the same PDMS prepolymer on a 4" silicon wafer at 1250 rpm and curing at 65  $^{\circ}\text{C}$  for half an hour. The final thickness of the membrane was 100  $\mu\text{m}$ . The gas channel layer was permanently bonded on the membrane using oxygen plasma and then peeled off from the wafer. A complete microfluidic chip was built after bonding the liquid channel layer with the gas layer/membrane composite. Alignment between the liquid channel and the relevant gas channel was conducted under a microscope. The dimensions of each valve were 600  $\mu\text{m}$  in diameter, 48  $\mu\text{m}$  in depth and 150  $\mu\text{m}$  across the valve seat. The liquid channel and the gas channel were 300 and 100  $\mu\text{m}$  in width, respectively. A three-layer notch valve with two notches can be seen in figure 2. In the case of double-notch ST valve, each notch measured 75  $\mu\text{m}$  in width and 4.66  $\mu\text{m}$  in depth.

For the ST valve, the major force that decelerates or retains the air/liquid interface is surface tension. According to Young's equation, the pressure to retain an air/liquid interface in a rectangular channel is expressed as

$$P_d = \frac{2(h + w)\sigma \cos(\pi - \theta_c)}{hw}, \quad (1)$$

where  $\theta_c$  is the contact angle of the liquid on a PDMS surface,  $\sigma$  is the surface tension of the liquid,  $h$  and  $w$  are the height and width of the notch, respectively. The retaining pressure

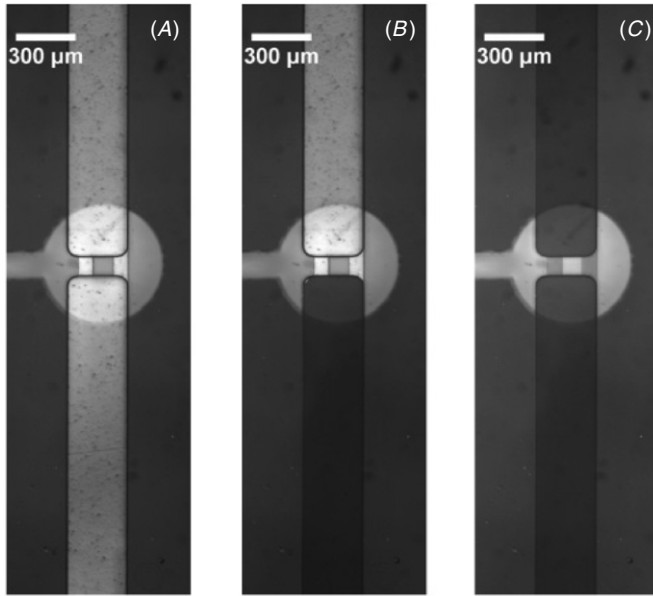


**Figure 2.** (a) Image of a double-notch ST valve with trapped air phase. (b) The interface is retained at the notch when the driving pressure is less than the threshold. (c) The liquid leaks through the notch when the pressure exceeds the threshold.

is related to the contact angle of liquid and the size of notch. Usually a hydrophobic material, such as PDMS, accompanied with a tiny channel can create a higher surface-tension force. For instance, the theoretical threshold pressure in a PDMS channel ( $\theta_c = 100^\circ$ ) with two notches is 11.5 kPa. In theory, a notch can be designed to withstand different threshold pressure values by varying the cross-sectional area, yet a practical limit may exist due to the potential PDMS membrane deformation in the case of extremely shallow notches.

For the GP valve, air is squeezed to the grooves adjacent to the liquid channel through the PDMS membrane. Due to the porous nature of PDMS matrix, the elastomer allows gas molecules to slowly migrate in and out of the material, yet retains liquid inside the channel. In general, the permeation can withstand large pressure but needs longer time to remove gas compared with the ST valve. A model derived from the gas-permeation equation [10] can be used to predict the remaining permeation area as a function of time:

$$A(t) = WL_0 \exp \left[ \frac{\alpha P(p_2 - p_1)}{db} \frac{T}{273} \frac{76}{P_{\text{atm}}} t \right], \quad (2)$$

where  $\alpha$  is an empirical correction factor,  $P$  is the permeation of the material,  $p_1$  and  $p_2$  are the pressure values before and after the PDMS matrix,  $b$  is the thickness of the membrane,  $d$  is the depth of the channel,  $W$  is the channel width,  $L_0$  is the initial length of the gas in the channel and  $t$  is the elapsed time. Basically, the purging rate reduced exponentially and varied with the pressure difference ( $p_2 - p_1$ ), the thickness of the membrane and the inherent material properties. The process can be accelerated by increasing pressure difference or reducing membrane thickness in the current setup. The equation facilitates users to design a valve that can remove gas in a reasonable timeframe.

In addition to the two dominant equations above, some other forces might play minor roles in the purging actions.

For instance, the hydraulic resistance caused by the friction between channel walls and liquid molecules is proportional to the channel length and flow rate according to the Hagen–Poiseuille equation. The driving pressure is progressively depleted when a fluid travels a long distance or flows with a high velocity. In the current setup, however, the pressure loss is negligible ( $<100$  Pa) compared with the driving pressure. Moreover, the decrease in fluid velocity due to highly compressed air in the last stage of the purging process in the GP valve can further mitigate the pressure loss.

### Gas removal by surface tension

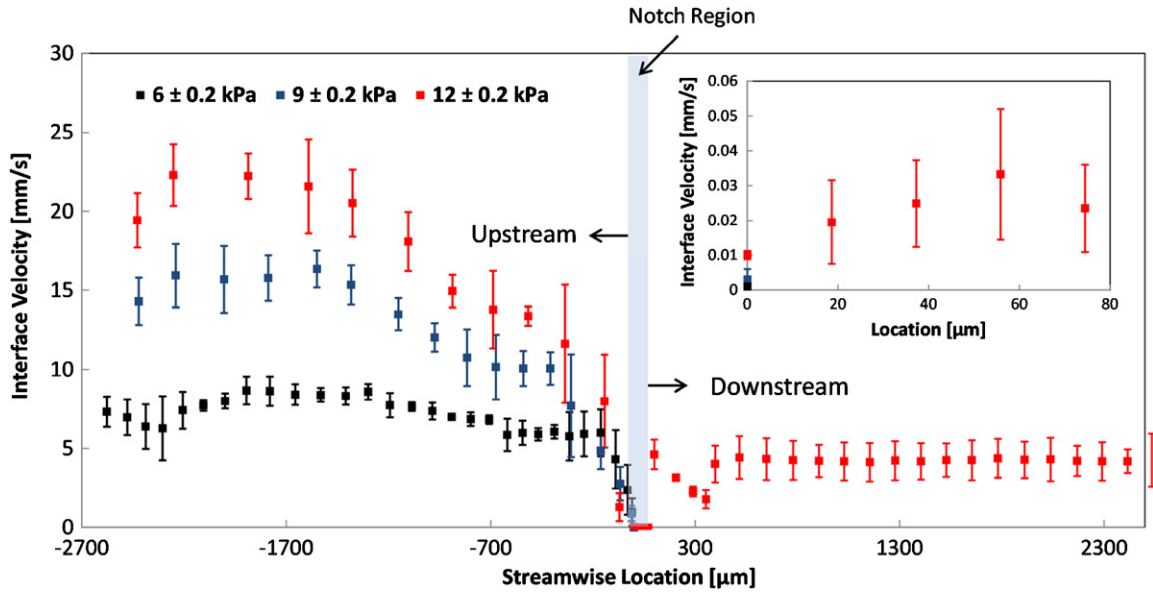
Both the purge valves, unless mentioned otherwise, were investigated in a closed state. A microchannel with input and output reservoirs and the ST valve were fabricated as per the previously described protocols. A water-based solution stained with a food color (ESCO Foods Inc.) was employed here as a working fluid and was placed in the input reservoir. The output reservoir was connected to a vacuum pump (Thomas Diaphragm Pump, 5002VD/1.0/N/DC) to create a driving force for fluid movement. The pump was connected to a dc power supply (Extech Instruments, 382260) and the pressure difference was controlled by adjusting the dc voltage. The set pressure values were observed to fluctuate between  $\pm 0.2$  kPa due to the motorized diaphragm pump.

Figure 2 demonstrates one of the experimental results for the double-notch ST valve. The leakage point was measured by varying the fluid driving pressure and was observed to reach a value around  $12 \pm 0.2$  kPa, which is close to the predicted threshold (11/5 kPa). It should be noted that some other factors, such as hydraulic resistance and contact-line pinning [4, 21], though minor in the current setup, may alter the threshold if the boundary condition is changed. Accordingly, the actual threshold may be higher than the theoretical value. The influences of both effects on the current thresholds are estimated to be less than 1%, respectively. To deal with the contact-line pinning, a measured contact angle should be used instead of a theoretical value. The alignment was found to be fast compared to the GP valve. The variation of the air/liquid interface velocity across the valve seat over location ( $x$ ) from the notch valve is shown in figure 3 (see supplementary movie (available at [stacks.iop.org/JMM/22/085023/mmedia](http://stacks.iop.org/JMM/22/085023/mmedia))). The start of the notch is located at the origin ( $x = 0$ ). Measurements upstream of the notch ( $x < 0$ ) as well as downstream of the notch ( $x > 0$ ) were recorded. The interface velocity drops to zero rapidly as the driving pressure is less than the threshold, whereas the interface slows down in the notch but resumes velocity after leaving the notch.

### Gas removal by permeation

Quantification of gas removal in the GP valve was also investigated. A series of experimental images showing the operation are depicted as insets in figure 4. Unlike the ST valve, excessive air is removed through the porous PDMS matrix with higher pressure acting on the liquid. Although the





**Figure 3.** Plot of the air/liquid interface velocities under three driving pressure conditions. The interface stops at the notch at low pressure ( $6 \pm 0.2$  kPa and  $9 \pm 0.2$  kPa), but leaks through the notch at driving pressure ( $12 \pm 0.2$  kPa) higher than the threshold. The inset shows a close-up of the interface velocity measured in the notch region ( $0 \leq x \leq 100$ ).

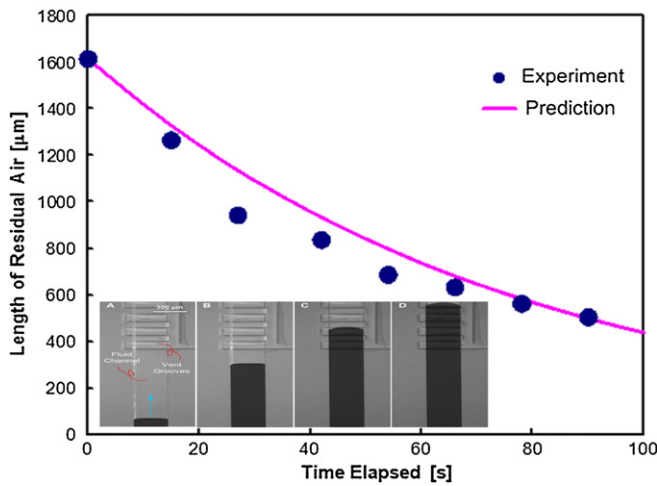


**Figure 4.** Comparison of the analytical prediction and the experimental measurement. The channel width and depth are fixed; therefore the volume of the residual air between the valve seat and the air/liquid interface is simplified to the change of length. The inset images from left to right represent the air/liquid interface at different time steps: (a) 0 s (b) 20 s (c) 40 s (d) 65 s.

GP valve is designed for high pressure, the purging process is time-consuming. According to equation (2), the purging time is proportional to the contact area with air. The purging efficiency drops significantly when less air remains in the channel (i.e. decrease in the contact area). In addition to the hydraulic resistance, the highly compressed air in the last stage may in part contribute to the decline of the efficiency. Air in front of a fluid is compressed initially due to low density but becomes more incompressible as the air density escalates. The process can be accelerated by increasing either the driving pressure or reducing the membrane thickness. The GP valve is equipped with vent grooves adjacent to a liquid channel, so that the pressure difference is increased. The finger-like

geometry is adopted here to extend the contact area in the last stage and prevent collapse of the structure. All of the aforementioned factors contribute to the acceleration during the purging process of the GP valve. The analytical model shows good agreement with the experimental data when  $\alpha$  is 13 and a pressure difference of 38 kPa is applied (figure 4).

### Evaluations of the GP valve in a microchannel

The GP valve was incorporated into a microchannel for some operating tests. The driving force was generated by an on-chip peristaltic pump. Four parameters were evaluated based on their influence on the displacement and fluid velocity. The results are discussed as follows.

- (i) *Pressure difference.* This section shows the comparison of purge valves with and without an upstream pressure source. The upstream pressure was generated from an on-chip peristaltic pump. When the pump was idle, the liquid moved slowly due to the low-pressure difference from the vacuum filled grooves. However, the purging accelerated while the pump was activated. The pump was able to provide a time-averaged pressure value of several tens of kilo-Pascals. A three-fold saving in time was observed when a pump was used (figure 5(A)). The corresponding velocities are shown in figure 6(A). Flow driven by the pump moved faster during the purging process. On average, the pump-driven flow maintained a mean velocity three-fold higher than the pumpless flow. Without a driving force, the flow lost its momentum and became stagnant at the last vent groove. In contrast, the pump-driven flow kept moving till it approached the valve seat.
- (ii) *Location of the liquid plug.* The purging rate is also subjected to the location of air/liquid interface. The

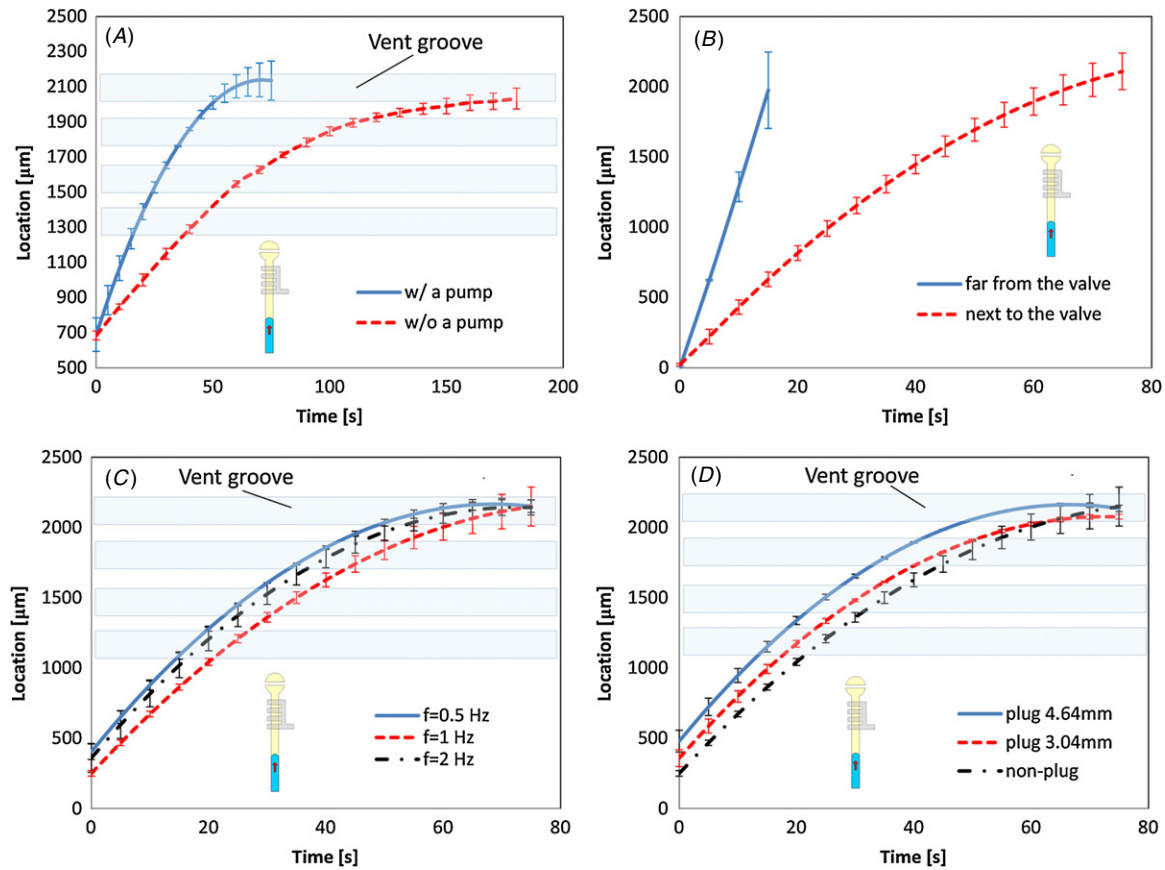


**Figure 5.** Displacement of liquid plug as a function of time. The blue stripes stand for the relative positions of vent grooves in the microchannel. (A) Purging with and without a pump. (B) Purging upstream (far away from the purge valve) and downstream (next to the purge valve). (C) Purging with different pumping frequencies. (D) Purging with different lengths of liquid plug.

purging efficiencies in the upstream ( $\sim 9.28$  mm away from the purge valve) and downstream (next to the purge valve) regions were measured (figure 5(B)). Upstream, the liquid moved relatively fast ( $\sim 132.72 \pm 39.69 \mu\text{m s}^{-1}$ ) owing to abundant air as a cushion as well as a large contact area in the microchannel. However, the air cushion appeared to be unreliable, resulting in velocity fluctuations in this region. In general, air is more compressible initially and becomes less compressible after being highly squeezed when the pumping rate is higher than the purging rate. The porous PDMS walls are necessary for promoting the purging process. However, this effect decreases exponentially according to the permeation equation (equation (2)). In the last stage, hydraulic resistance depletes only some of the driving pressure ( $< 100$  kPa). Also, the air compressibility and contact area of channel walls play minor roles in the purging process. The vent grooves therefore become the only exit for the excessive air, resulting in a decline in the flow velocity (figure 6(B)). This unique characteristic makes the processing time escalate when an air/liquid interface moves near the GP valve.

(iii) *Pumping frequency.* Changing the pumping frequency is a major means for a peristaltic pump to vary flow velocity. In principle, a higher pumping frequency results in faster fluid flow. To characterize the relationship,

the velocities subjected to three frequencies, 0.5, 1 and 2 Hz, were measured. As shown in figures 5(C) and 6(C), no meaningful difference is observed between the frequencies considering the rate of change of displacement as well as velocity. All of the linear correlation coefficients between any two cases are higher than  $R^2 = 99.4\%$ , implying very similar trends. The cause is attributed to the highly compressed air in the last stage and the nature of the peristaltic pump. As discussed in the previous sections, the flow velocity declined on approaching the GP valve due to slow permeation. The compressed air caused backpressure when excessive pressure was accumulated in the channel between the air/liquid interface and the valve seat. Since the accumulated pressure was usually stronger than the frequency change by the peristaltic pump, no significant improvement in velocity was measured even though the frequency was increased. The excessive pressure then released back to the pump, decreasing the pumping efficiency. This situation occurs in different phases depending on different pumping sequences. However, the phenomenon becomes negligible when the air/liquid interface remains far away from the purge valve.

(iv) *Length of the liquid plug.* The last parameter shows the influence resulting from the length of the liquid plug. A liquid plug is essential when metering or quantification

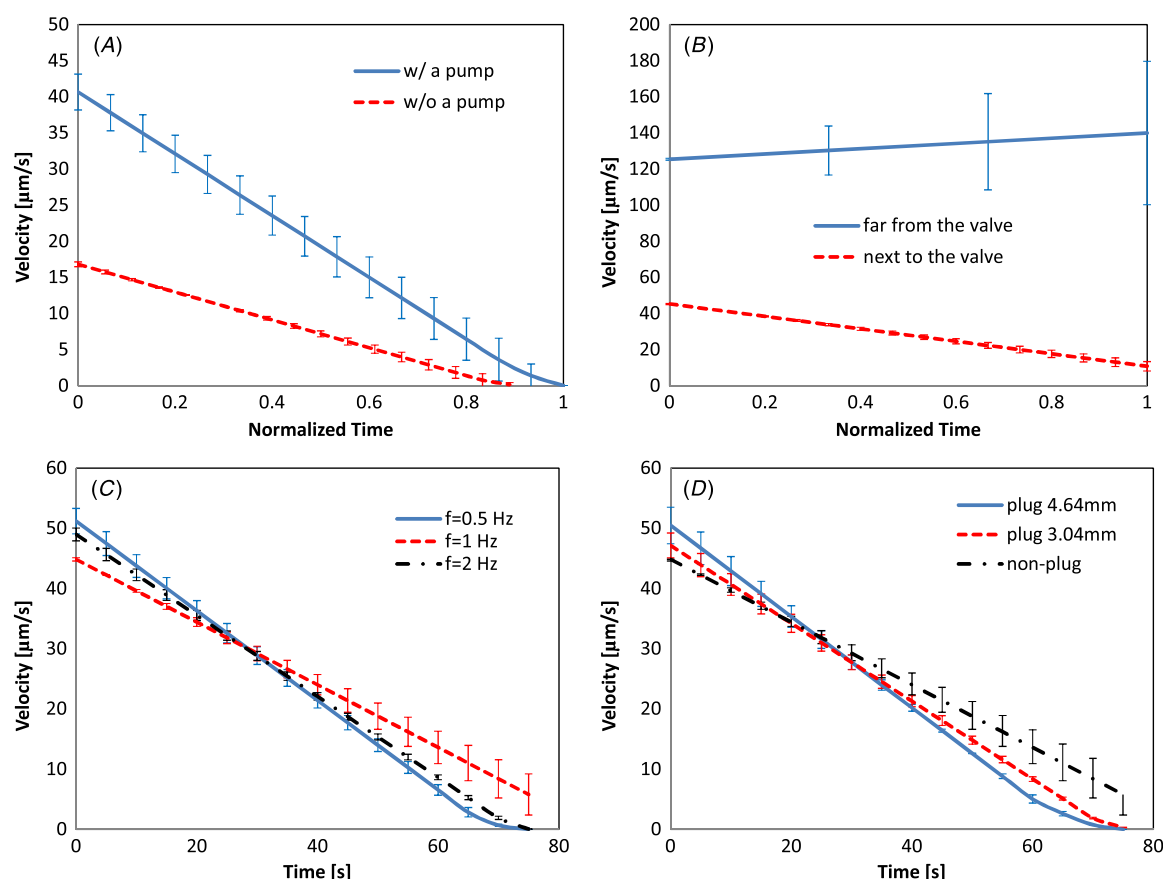


**Figure 6.** Flow velocity as a function of location. (A) Purging with and without a pump. (B) Purging upstream (far away from the purge valve) and downstream (next to the purge valve). (C) Purging with different pumping frequencies. (D) Purging with different lengths of liquid plug.

is required. A non-plug fluid and two plugs measuring 3.04 and 4.64 mm in length were compared under the same conditions. As shown in figures 5(D) and 6(D), the purging appears to be independent of the length of the liquid plug. There are no distinguishable differences in the liquid displacement as well as the velocity. Similar to the previous pumping frequency, the minimal correlation coefficient is  $R^2 = 99.2\%$ , implying the same behavioral pattern. This result implies that the hydraulic resistance due to the friction between the liquid and the solid walls is negligible as the air/liquid interface is very close to the purge valve (slow velocity). In other words, only gas permeation dominates the purge process in the last stage.

### Liquid alignment for rapid mixing

Manipulation of liquid alignment before mixing in a microfluidic chip using GP valves was performed. As shown in figure 7, two liquid plugs stained with different food colors were used to facilitate the visual observation. To minimize human errors, the operations were automated with a self-developed LabVIEW® (National Instruments) program. In the chip, the plugs were translated by peristaltic pumps. The pump was composed of three normal Mathies' valves

**Table 1.** Mixing efficiency at different mixing cycles.

	Zeroth cycle	First cycle	Second cycle	Third cycle	Fourth cycle
Efficiency (%)	$41.88 \pm 13.21$	$94.28 \pm 3.92$	$93.14 \pm 5.64$	$94.38 \pm 4.16$	$94.49 \pm 3.81$

and operated in an orderly fashion. The details regarding the pump and the chip were discussed in the relative papers [1, 2]. For the mixing, the green plug was first translated to a designated location (figures 7(A)–(C)) and so was the red plug (figures 7(D)–(E)). Without actively sensing, the alignment was achieved by pumping both the liquid plugs for a certain period of time till they approached the valve seats. The time required for each alignment was calibrated in advance and was estimated to be shorter than 1.5 min. After both plugs were well aligned (figure 7(F)), the valves were opened simultaneously and both plugs were squeezed into the third channel for chaotic mixing (figure 7(G)). Figures 7(H) and (I) show the statuses of the mixture at the first cycle and the second cycle, respectively. The insets in figures 7(H) and (I) indicate the completion of the mixing. Note that a fluorescent dye was added in one of the liquid plugs during the quantification of mixing efficiency (see supplementary material (available at [stacks.iop.org/JMM/22/085023/mmedia](http://stacks.iop.org/JMM/22/085023/mmedia)) for details). The

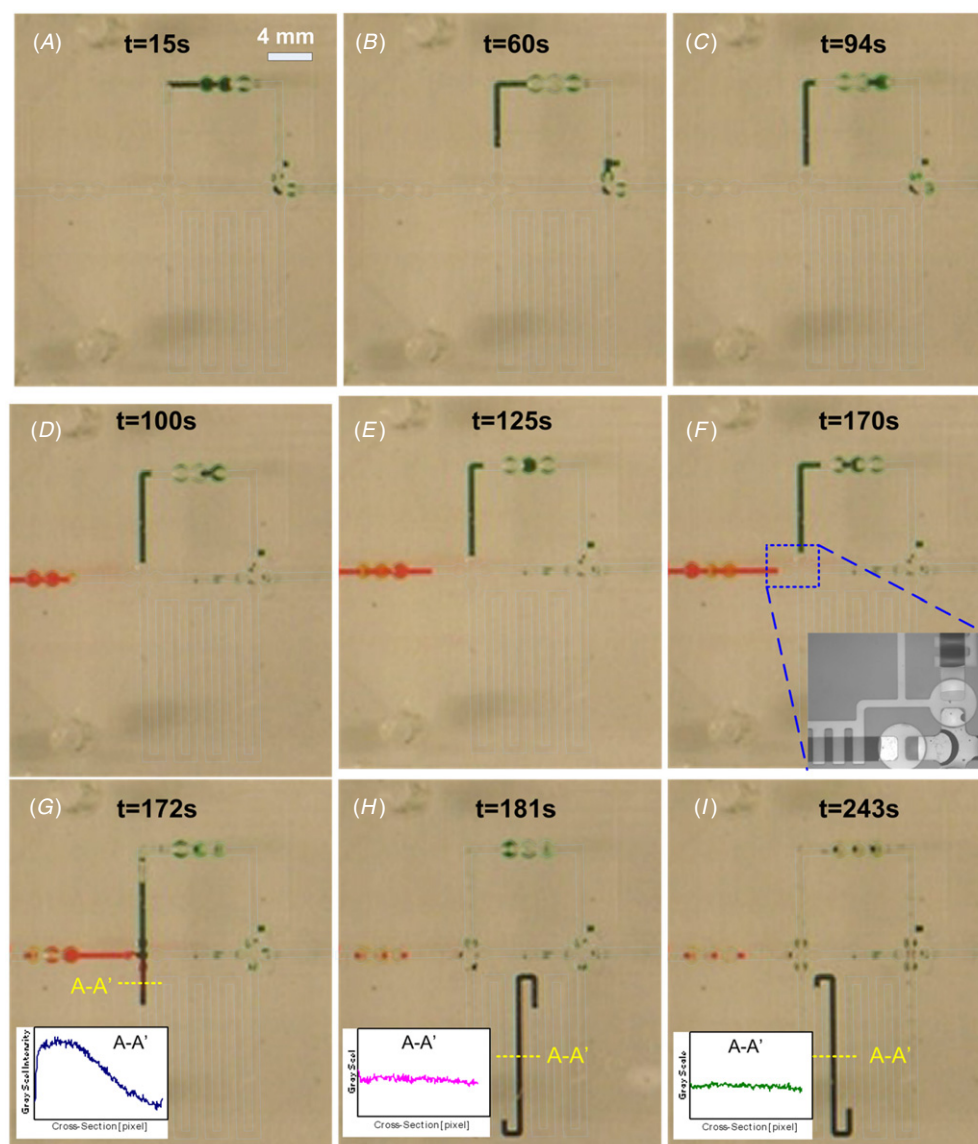


**Figure 7.** A series of experimental images demonstrating the rapid liquid mixing in microchannels. (A)–(F) Two different food colors are aligned and then sent to a third channel for mixing. The alignment for each plug takes about 80 s. (G)–(I) Without the obstruction of air bubbles, the mixing is completed rapidly within two cycles (see the supplemental file (available at [stacks.iop.org/JMM/22/085023/mmedia](http://stacks.iop.org/JMM/22/085023/mmedia))). The insets in images (G)–(I) illustrate the mixing profiles at different stages.

complete mixing was achieved rapidly after the first cycle without air bubbles or air gaps between plugs. A list of the mixing efficiency from the beginning to the fourth cycle is shown in table 1. The definition of the efficiency can be referred to the prior literature [22]. The mixing efficiency (mean  $\pm$  standard deviation) is poor before the liquid plug starts running loops. However, it swiftly exceeds 90% and reduces uncertainty after the first cycle. The results confirm that rapid mixing could be realized with the deployment of the purge valves. Compared with other mixing strategies reported in the literature [15, 16, 20], the mixing rate of the current device at  $Re = 0.32$  is 0.2. This mixing rate is very competitive among the existing techniques. The rapid mixing capability is obtained from breaking continuous flow into liquid plugs, therefore sharing the same mechanism with the so-called droplet mixing in the digital microfluidics.

## Conclusion

Two types of unique gas purge valves eligible for two distinct pressure ranges are presented in this study. The proposed devices not only work as a gateway for normal flow controls but also remove excessive air for liquid alignment without active sensing elements. The ST valve can either retain liquids with small pressure ( $<11.5$  kPa) or slow down fluid flow when the driving pressure exceeds the threshold. The functional mechanism of the ST valve is the surface tension induced by hydrophobic channel walls. The analytical threshold is 11.5 kPa under the current setup. In contrast, the mechanism that drives the GP valve is gas permeation based on the porosity of PDMS. Finger-like grooves deployed adjacent to a liquid channel are connected to vacuum to remove excessive air. The employment of PDMS membrane allows the GP valve to be operated with higher pressure



(>5.5 kPa). According to the permeation equation, high pressure accelerates the purging process. Additionally, the GP valve was evaluated with four parameters. The purging rate varied with the location of air/liquid interface as well as the pressure difference (i.e. a pump in this case). The interface velocity was high when the liquid remained far away from the purge valve or the pressure difference across the PDMS membrane was increased. Hydraulic resistance may alter the efficiency as well. However, the effect was estimated to be negligible in the current setup. Surprisingly, the pumping frequency and the length of liquid plug showed no significant influence on the purging rate. The results suggested that gas permeation primarily dominates the purging process as the liquid approaches the purge valve. Eventually, a demonstration of rapid mixing using the GP valves showed a practical application. Since air bubbles were not trapped between liquid plugs, the mixing was rapidly completed after only one cycle. The deployment of purge valves in microfluidic chips is believed to benefit lab-on-a-chip applications.

## Acknowledgments

The authors thank the National Science Council grant 100-2218-E-006-036 for supporting this work. The authors also acknowledge the technical support from Birk Nanotechnology Center at Purdue Discovery Park.

## References

- [1] Amin A M, Thottethodi M, Vijaykumar T N, Wereley S T and Jacobson S C 2007 A general-purpose architecture for programmable microfluidics *11th Int. Conf. on Miniaturized Systems for Chemistry and Life Sciences, microTAS*
- [2] Chuang H S, Amin A M, Thottethodi M, Vijaykumar T N, Wereley S T and Jacobson S C 2008 Polydimethylsiloxane (PDMS) peristaltic pump characterization for programmable lab-on-a-chip applications *12th Int. Conf. on Miniaturized Systems for Chemistry and Life Sciences, microTAS (San Diego, LA, USA)* [http://www.rsc.org/binaries/LOC/2008/PDFs/Papers/564\\_0154.pdf](http://www.rsc.org/binaries/LOC/2008/PDFs/Papers/564_0154.pdf)
- [3] Cole M C and Kenis P J A 2009 Multiplexed electrical sensor arrays in microfluidic networks *Sensors Actuators B* **136** 350–8
- [4] Forsberg P S H, Priest C, Brinkmann M, Sedev R and Ralston J 2010 Contact line pinning on microstructured surfaces for liquids in the Wenzel state *Langmuir* **26** 860–5
- [5] Grover W H, Ivester R H C, Jensen E C and Mathies R A 2006 Development and multiplexed control of latching pneumatic valves using microfluidic logical structures *Lab Chip* **6** 623–31
- [6] Grover W H, Skelley A M, Liu C N, Lagally E T and Mathies R A 2003 Monolithic membrane valves and diaphragm pumps for practical large-scale integration into glass microfluidic devices *Sensors Actuators B* **89** 315–23
- [7] Hosokawa K, Fuji T and Endo I 1999 Droplet-based nano/picoliter mixer using hydrophobic microcapillary vent *MEMS'99: 12th IEEE Int. Conf. on MEMS* pp 388–93 [http://ieeexplore.ieee.org/xpls/abs\\_all.jsp?arnumber=746860&tag=1](http://ieeexplore.ieee.org/xpls/abs_all.jsp?arnumber=746860&tag=1)
- [8] Huang C W, Huang S B and Lee G B 2008 A microfluidic device for precise pipetting *J. Micromech. Microeng.* **18** 035004
- [9] Kang J H, Kima Y C and Park J K 2008 Analysis of pressure-driven air bubble elimination in a microfluidic device *Lab Chip* **8** 176–8
- [10] Kang J H, Kima Y C and Park J K 2008 Analysis of pressure-driven air bubble elimination in a microfluidic device *Lab Chip* **8** 176–8
- [11] Lee S H, Lee C S, Kim B G and Kim Y K 2003 Quantitatively controlled nanoliter liquid manipulation using hydrophobic valving and control of surface wettability *J. Micromech. Microeng.* **13** 89–97
- [12] Mata A, Fleischman A J and Roy S 2006 Fabrication of multi-layer SU-8 microstructures *J. Micromech. Microeng.* **16** 276–84
- [13] Shin Y S, Cho K, Lim S H, Chung S, Park S J, Chung C, Han D C and Chang J K 2003 PDMS-based micro PCR chip with parylene coating *J. Micromech. Microeng.* **13** 768–74
- [14] Srivastava N and Burns M A 2006 Electronic drop sensing in microfluidic devices: automated operation of a nanoliter viscometer *Lab Chip* **6** 744–51
- [15] Stone Z B and Stone H A 2005 Imaging and quantifying mixing in a model droplet micromixer *Phys. Fluids* **17** 063103
- [16] Teh S Y, Lin R, Hung L H and Lee A P 2008 Droplet microfluidics *Lab Chip* **8** 198–220
- [17] Tseng H Y, Wang C H, Lin W Y and Lee G B 2007 Membrane-activated microfluidic rotary devices for pumping and mixing *Biomed. Microdevices* **9** 545–54
- [18] Unger M A, Chou H P, Thorsen T, Scherer A and Quake S R 2000 Monolithic microfabricated valves and pumps by multilayer soft lithography *Science* **288** 113–6
- [19] Urbanski J P, Thies W, Rhodes C, Amarasinghe S and Thorsen T 2006 Digital microfluidics using soft lithography *Lab Chip* **6** 96–104
- [20] Voth G A, Saint T C, Dobler G and Gollub J P 2003 Mixing rates and symmetry breaking in two-dimensional chaotic flow *Phys. Fluids* **15** 2560–6
- [21] Walker S W and B S 2006 Modeling the fluid dynamics of electro-wetting on dielectric (EWOD) *J. Microelectromech. Syst.* **15** 986–1000
- [22] Yang R-J, Wu C-H, Tseng T-I, Huang S-B and Lee G-B 2005 Enhancement of electrokinetically-driven flow mixing in microchannel with added side channels *Japan. J. Appl. Phys.* **44** 7634–42